

Geophysical Research Letters

RESEARCH LETTER

10.1029/2020GL090836

Key Points:

- We resolve the mechanisms driving thick salt layers accretion in deep saline waterbodies by direct field measurements in the Dead Sea
- Hydroclimatic variations impact stratification stability, thermohaline staircases, double diffusion salt fluxes, and halite deposition
- Regional and seasonal drying trends dictate stronger salt flux in the drier and deeper zones and explain the architecture of "salt giants"

Supporting Information:

- · Supporting Information S1
- · Table S1

Correspondence to:

N. G. Lensky, nadavl@gsi.gov.il

Citation:

Sirota, I., Ouillon, R., Mor, Z., Meiburg, E., Enzel, Y., Arnon, A., & Lensky, N. G. (2020). Hydroclimatic controls on salt fluxes and halite deposition in the Dead Sea and the shaping of "salt giants". *Geophysical Research Letters*, 47, e2020GL090836. https://doi.org/10.1029/2020GL090836

Received 17 SEP 2020 Accepted 26 OCT 2020 Accepted article online 29 OCT 2020

Hydroclimatic Controls on Salt Fluxes and Halite Deposition in the Dead Sea and the Shaping of "Salt Giants"

Ido Sirota^{1,2} D, Raphael Ouillon³ D, Ziv Mor^{1,2}, Eckart Meiburg³ D, Yehouda Enzel¹ D, Ali Arnon² D, and Nadav G. Lensky² D

¹The Fredy and Nadine Herrmann Institute of Earth Sciences, The Hebrew University of Jerusalem, Jerusalem, Israel, ²Geological Survey of Israel, Jerusalem, Israel, ³Department of Mechanical Engineering, University of California, Santa Barbara, CA, USA

Abstract As the only deep hypersaline, halite-precipitating lake on Earth today, the Dead Sea is the single modern analog for investigating the mechanisms by which large-scale and thick salt deposits, known as "salt giants", have accreted in the geological record. We directly measure the hydroclimatic forcing and the physical limnologic processes leading to halite sedimentation, the vertical thermohaline structure, and salt fluxes in the Dead Sea. We demonstrate that changes in these forcing lead to strong seasonal and regional variations in the stratification stability ratio, triggering corresponding spatiotemporal variations in thermohaline staircase formation and diapycnal salt flux, and finally control the thickness of the halite layer deposited. The observed staircase formation is consistent with the mean-field γ instability, causing layering in double-diffusive convection. We show that double diffusion and thermohaline staircase formation drive the spatial variability of halite deposition in hypersaline water bodies, underlying and shaping "salt giants" basin architecture.

Plain Language Summary Kilometers-thick halite sequences in the geological record represent some of the extreme environmental events during Earth's history. The present-day Dead Sea serves as an analog for halite deposition and the unique limnology/oceanography of those past hypersaline environments. We observe differential downward salt flux in the lake and halite deposition at the deep lakefloor, corresponding to theoretical requirements of water column stability and the evolution of a step-like thermohaline structure of the water column. These variations are spatiotemporally controlled by regional hydroclimatology, as the salt flux and halite deposition enhanced during the dry summer and farther from the freshwater inflows into the lake, along an increasing salinity gradient. Our findings explain thick halite accretion in global basin depocenters.

1. Introduction

Kilometer-thick halite sequences were accreted throughout Earth's geological history (Hsü et al., 1973; Kozary et al., 1968; Ronov et al., 1980) in deep hypersaline basins (Hardie & Lowenstein, 2004; Hsu, 1972; Schmalz, 1969), during extreme dry episodes (Hsu, 1972; Warren, 2010) and under spatial hydroclimatic gradients (Karakitsios et al., 2017; Simon & Meijer, 2017). The mechanisms forming these salt giants have been the focus of a longstanding debate (Hsu, 1972; Roveri, Manzi, et al., 2014; Schmalz, 1969; Simon & Meijer, 2017). Evaporation from halite-saturated brine drives evaporitic deposition (Hsu, 1972; Lowenstein & Hardie, 1985; Schmalz, 1969); however, mass balance arguments alone cannot explain the observed spatial variations in thickness (Hsu, 1972; Meijer & Krijgsman, 2005), the required deposition rates (Hsu, 1972; Schmalz, 1969), and the basin architecture of these salt giants (Flecker et al., 2015; Kirkham et al., 2020; Meijer & Krijgsman, 2005). Evaporation at the surface of deep hypersaline basins sets in motion, intricately coupled mechanisms involving the diffusive and convective transport of heat and dissolved salt, driving halite deposition on the basin floor (Arnon et al., 2016; Sirota et al., 2016, 2017). Our data-rich observations were conducted for the Dead Sea (Figures 1a and 1b), the only modern analog of deep hypersaline basins (Arnon et al., 2016; Kirkham et al., 2020; Sirota et al., 2016, 2017, 2018). This deep (~290 m), perennial, hypersaline lake actively deposits thick halite units in response to negative water balance (Lensky et al., 2005; Sirota et al., 2017; Steinhorn, 1983; Stiller et al., 1997); the lake is Ca-Cl rich compared to evaporated ocean

©2020. American Geophysical Union. All Rights Reserved.

SIROTA ET AL. 1 of 10

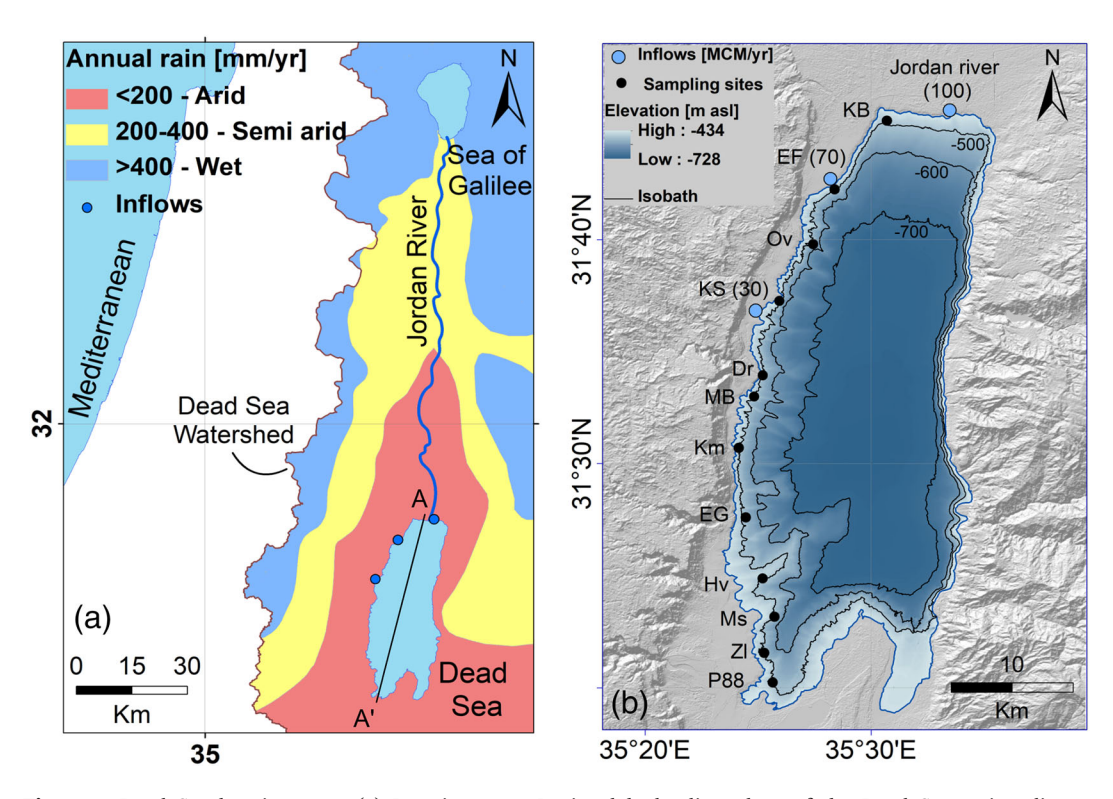


Figure 1. Dead Sea location map. (a) Location map. Regional hydroclimatology of the Dead Sea region dictates hydrological forcing gradient from north to south. Main freshwater inflows into the lake are located at its northern end. (b) Main freshwater inflows into the Dead Sea (blue circles) form a surface water salinity gradient; surface salinity increases southward. Sampling sites in this study (black dots).

water, and its composition changes, for example, decrease of Na/Cl ratio, with halite deposition (Gavrieli et al., 2011). Regional hydroclimatic gradient (Mor et al., 2018) over the lake surface is imposed by inflows at the humid northern end, whereas the southern end is subjected only to evaporation (Figures 1b and 2a). In addition, seasonal temperature variations superimposed on the continuously negative water balance (Figure 2b) instigates stable thermohaline stratification during summers, characterized by a warmer and saltier upper layer above a colder, less saline lower layer (Anati et al., 1987; Arnon et al., 2016; Steinhorn, 1985). This configuration triggers double-diffusive fingering, an instability that evolves in stably stratified environments where two scalars contribute to the density in opposite ways, and diffuse at different rates (Stern, 1960; Turner, 1974). In the Dead Sea, heat is the stabilizing fast diffuser, while salinity is the destabilizing, slow diffuser (Anati & Stiller, 1991; Arnon et al., 2016; Ouillon et al., 2019). Linear stability theory (Radko, 2013) indicates that the emergence of double-diffusive fingering depends on the stratification stability (density) ratio $R_{\rho} = \frac{\alpha T_z}{\beta S_z}$ (Figure 2c), that is, the relative contributions of temperature and salinity in determining the vertical density gradient, where T_z and S_z denote the vertical temperature and salinity gradients, respectively, with α and β being the thermal and salinity expansion coefficients. The coefficients k_S and k_T represent salt and heat diffusivities, and the diffusivity ratio is τ

 $=\frac{k_S}{k_T}$ 0.01. The stratified system is unstable to the double-diffusive fingering instability when $1 < R_{
ho} < \frac{1}{\tau}$; such a system, interestingly, generates a faster convective downward flux, from the epilimnion to the hypolimnion, of the slow diffuser (dissolved salt) compared with a slower flux of the fast diffuser (heat flux) (Arnon et al., 2016; Ouillon et al., 2019), that is, $\frac{F_T}{F_S} < 1$, where F_T and F_S are the downward heat and salt flux, respectively. Hence, the fingering regime reduces halite saturation at the epilimnion leading to undersaturation, while maintaining supersaturation and halite deposition at the hypolimnion (Ouillon et al., 2019; Sirota et al., 2016). Halite deposition at the hypolimnetic lakefloor (Sirota et al., 2017) slightly

SIROTA ET AL. 2 of 10

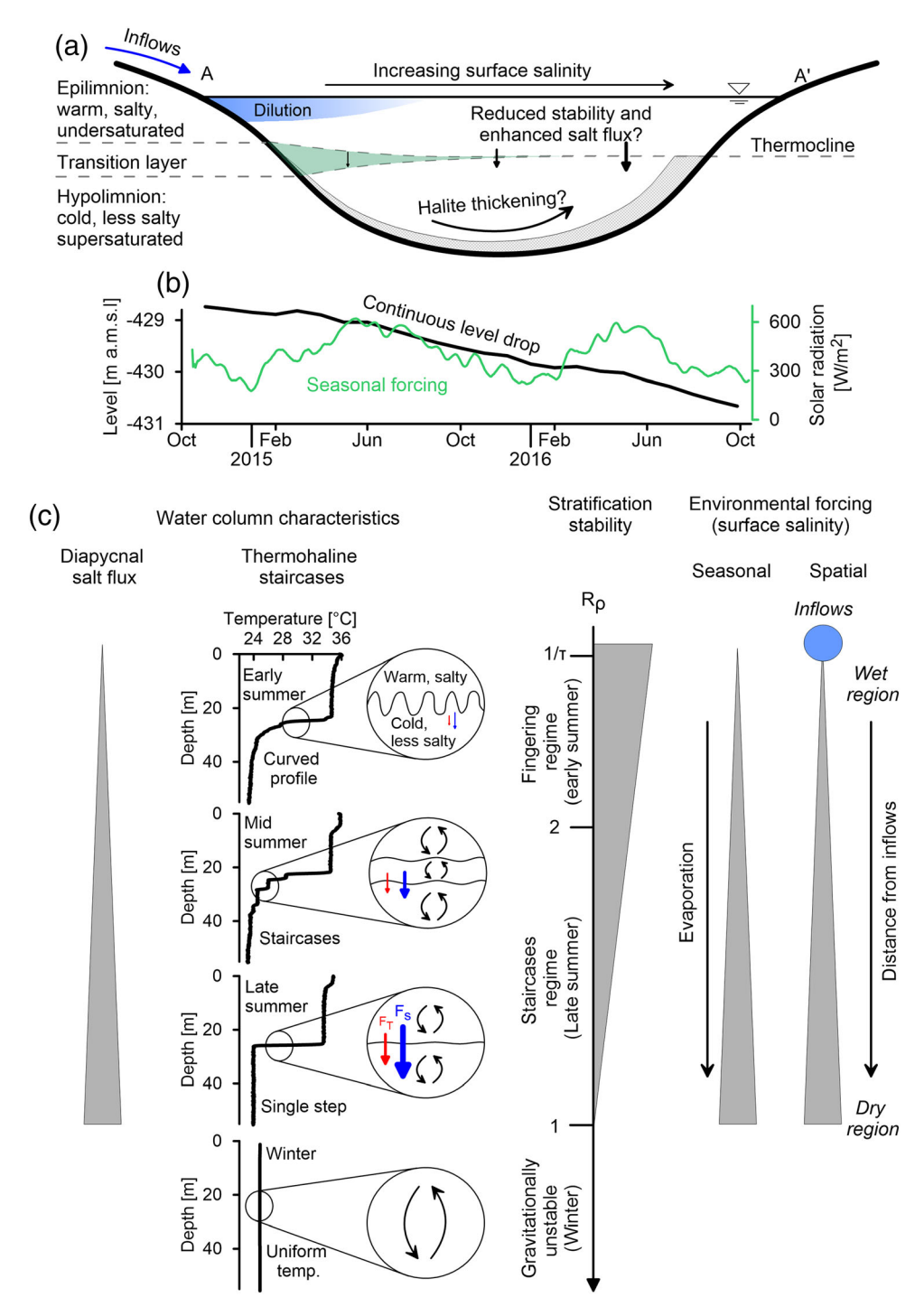


Figure 2. Environmental settings of the Dead Sea. (a) The regional hydroclimatic forcing-hypothetical illustration of horizontal depth variations across the Dead Sea (A-A' transect), in response to the hydrological gradient. The inflows imposed horizontal salinity gradient that drives variations in the water column properties from north to south. We hypothesize stronger downward salt flux and halite deposition farther from the inflows. (b) The seasonal hydroclimatic forcing-annual level decline and solar radiation (daily averaged) in the Dead Sea. (c) Water column characteristics in response to the seasonal and horizontal hydroclimatic forcing. Stratification stability, reflected by R_{ρ} , is reduced with surface salinity increase during the summer and farther from the freshwater inflows, toward the dry regions. The reduced stability leads to the development of thermohaline staircases and to an enhanced diapycnal salt flux during the summer. F_S and F_T are the downward salt and heat flux, respectively. Temperature depth profile during the entire stratification period does not display inversions; thus, lateral intrusions of fresher and colder water by inflows are not expected to impact on the double-diffusive mixing in the Dead Sea.

SIROTA ET AL. 3 of 10



reduces the salinity of the residual brine (reduction of ~0.1% from the total salinity, (Sirota et al., 2016)), leading to upward buoyancy flux that mixes the hypolimnion, but does not impact on the thermocline and the overlying epilimnion. The Dead Sea field data further indicate that the transition layer is organized in a form of thermohaline staircases, where the temperature and salinity of the layers decrease with depth, and over time the layers gradually merge (Figure 2c). Qualitatively similar staircasing has been observed in the ocean for R_{ρ} < 2 (Radko, 2003; Schmitt, 1981; Zodiatis & Gasparini, 1996). Theory (Radko, 2003, 2013) and numerical simulations (Stellmach et al., 2011; Traxler et al., 2011) link this staircases formation to the growth of a secondary mean-field instability, the so-called γ instability, which results in dramatically increased turbulent heat and salt fluxes. Elsewhere, such as in polar and tropical oceans (Ruddick & Richards, 2003) and laboratory experiments (Ruddick et al., 1999; Ruddick & Turner, 1979), it was proposed that thermohaline staircases are due to lateral sheared advection across lateral water mass gradients (Ruddick & Ruddick & Kerr, 2003; Simeonov & Stern, 2004, 2007). The signature of such lateral intrusions, however, is inversions in temperature and salinity with depth, which are not observed in the Dead Sea. In this lake, staircases display a monotonic decrease in temperature and salinity with depth (Arnon et al., 2016; Sirota et al., 2016), thus eliminating lateral thermohaline intrusion as a potential mechanism. Here, we analyze the Dead Sea field observations of thermohaline staircases from the perspective of double-diffusive instabilities, to quantify the role of hydroclimatology on thermohaline staircases and to identify the origins behind spatial variations in the architecture of salt giants in deep hypersaline basins.

2. Methods

A summer (27–29 July 2015) offshore survey was conducted to determine the limnological variations along the water column across the north-south transect, at 12 sites (see map in Figures 1b and 3).

2.1. Water Column Characterization

Temperature depth profiles were measured using CTD casts (SBE19, Seabird, USA). Salinity cannot be determined by conductivity sensors due to the high ionic strength of the Dead Sea brine; thus, salinity is determined by means of densitometry, which requires water sampling using Niskin bottles (General Oceanics, USA) at various depths. Accurate density and quasi-salinity measurements were performed in the laboratory (DMA 5000, Anton Paar, Austria) at 30°C, at an accuracy of 0.005 kg/m³, following the standard Dead Sea procedure (Gertman & Hecht, 2002; Sirota et al., 2016). The salinity values reported here are in sigma units (density excess over 1,000 in kg/m³). The equation of state for the Dead Sea brine is approximated by a linear equation (Ouillon et al., 2019) with thermal expansion coefficient $\alpha = -0.45$ kg/m³/°C (Gertman et al., 2010) and the saline expansion coefficient is $\beta = 0.936$ kg/m³/‰ (Anati et al., 1987).

2.2. Halite Crystallization Rates

The macroscopic rate of halite growth along the water column was inferred by in situ measurement, using a vertical steel cable hanging in the water column. The steel cable (5 mm thick) was anchored to the seafloor by a weight, at a water depth of 40 m and kept vertical by a tension buoy. The steel cable served as a platform for halite crystallization. The diameter of the cylindrical halite crystals coating around the 40-m-long cable was measured after 42 days at intervals of 1–5 m along the cable (Sirota et al., 2016). Halite crystallization rates were measured during the summer, at two sites simultaneously, one near the freshwater inflows in the northern part of the Dead Sea (EF) and the second at the southern part of the Dead Sea (Ms), ~30 km south from the inflows (see map in Figure 1b).

3. Results and Discussion

3.1. Hydroclimatic Controls of Seasonal and Regional Variations in Thermohaline Stratification and Halite Deposition

The seasonal evolution of the thermohaline stratification is dictated by the dry overall conditions and by the resulting negative water balance, on which the seasonal heat exchange is superimposed (Figure 2b). During the summer, evaporation from the lake surface, reflected by lake-level decline (~0.1 m/month, Figure 2b), raises surface salinity (e.g., from 241 to 244 kg/m³) and increases the salinity difference between the epilimnion and hypolimnion, that is, destabilizing halocline (from 0.4 kg/m³ in April to 3 kg/m³ in late July at Site EG, Figure 3a). During the same time interval, the temperature difference between the epilimnion and

SIROTA ET AL. 4 of 10

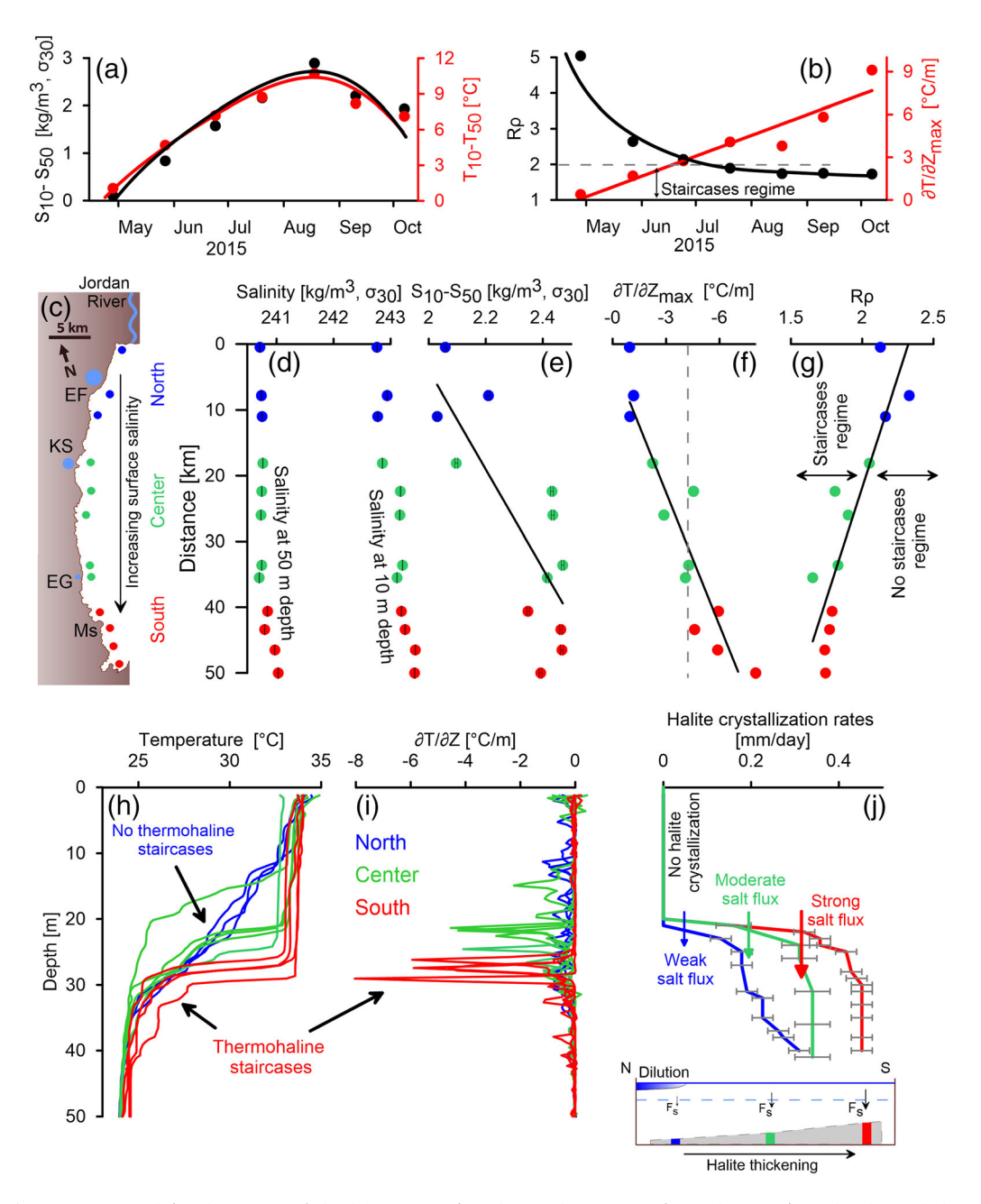


Figure 3. Seasonal (in the center of the lake, EG site) and spatial variations (at midsummer) in the thermohaline stratification. (a) Seasonal evolution of the difference in salinity (black) and temperature (red) between the upper and the lower layer. (b) The seasonal evolution of density ratio (black) and maximum vertical temperature gradient (red). (c) Sampling sites and location of freshwater inflows (blue circles) along the salinity gradient from north to south. (d) Salinity at 10- and 50-m depths from north to south. (e) Salinity depth difference between the upper (S₁₀: salinity at 10-m depth) and lower (S50: salinity at 50-m depth) layer from north to south. The increasing trend reflects the distance from freshwater inflows in the north. (f) The maximum vertical temperature gradient at each site from north to south. This trend reflects the development of thermohaline staircases in the southern region. (g) The density ratio at each location from north to south. Thermohaline staircases form when $R_{\rho} < 2$, as measured at central and southern sites of the lake, spatially correlated with sites of observed thermohaline staircases and enhanced salt flux. (h) Temperature depth profiles at 12 sites, displaying thermohaline staircase regime in the southern region and curved profiles in the northern region. At all sites, depth profiles display a monotonic temperature decrease with no inversions, thus excluding the impact of lateral intrusions on the staircases formation. (i) Vertical temperature gradient shows steps and depth of the thermocline at each site. (j) Halite crystallization rate along the water column exhibits southward increase below the thermocline, indicating enhanced downward salt flux from the upper saltier layer to the lower layer. Due to the supersaturation of the lower layer, the salt flux results in halite crystallization, and the accumulated halite layer thickens amplifies southward.

SIROTA ET AL. 5 of 10

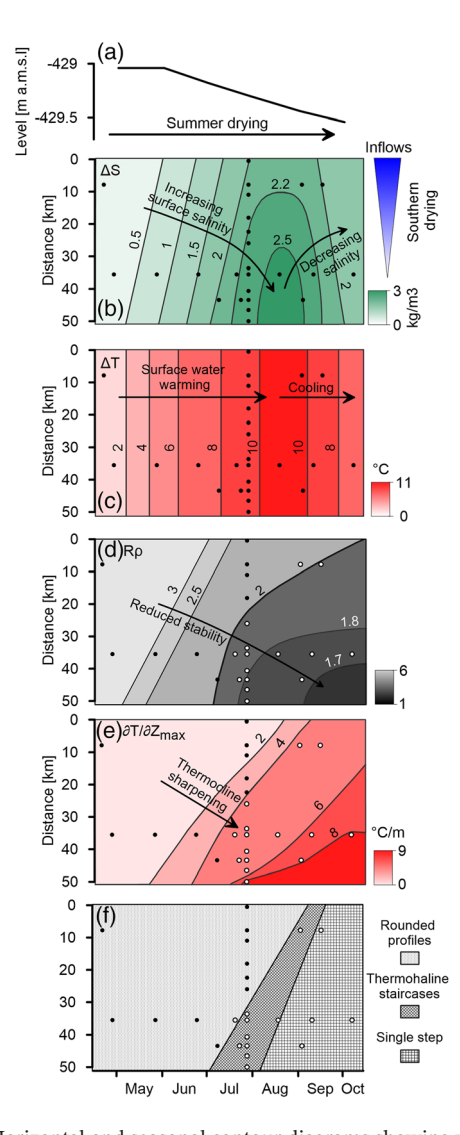


Figure 4. Horizontal and seasonal contour diagrams showing variations in the limnological characteristics of the Dead Sea water column during the summer and their environmental controls. The dots are measured or calculated data. (a) Seasonal forcing-continuous level decline during the summer due to the negative water balance leads to increasing salinity. (b) Salinity depth difference between the epilimnion (10 m) and hypolimnion (50 m). The salinity of the upper layer increases toward midsummer and southward. The reduction in the salinity of the upper layer during autumn is due to the downward salt fingering flux. (c) Temperature depth difference between the epilimnion (10 m) and hypolimnion (50 m). (d) Density ratio, calculated from the two measured variables presented in panels (b) and (c). The density ratio, which reflects water column stability, decreases during the summer and southward. Values below two support thermohaline staircase formation and significant fingering salt flux. White dots reflect places where measured temperature profiles display thermohaline staircases. The theoretical and observed fields are in good agreement with each other. (e) The maximum vertical temperature gradient increases at all sites during the summer, with the fastest increase occurring in the southern region. This reflects the more rapid evolution of the temperature profiles, from curved shapes to staircases that finally merge into a single step in the southern region. White dots reflect places where temperature profiles display thermohaline staircases. (f) Observed shape of temperature profile indicates the spatiotemporal field of thermohaline staircases. Observed thermohaline staircases are correlated with $R_o < 2$.

hypolimnion increases to ~11°C (Figure 3a), which corresponds to a stabilizing thermocline with density difference of ~5 kg/m³, enabling stable overall stratification. The Dead Sea is saturated with respect to halite; thus, the salinity rise due to negative water balance, is limited by the brine's temperature-dependent saturation (Sirota et al., 2016), and the deposition of halite provides an upper limit to the brine's salinity; thus the measured salinity closely match the saturation salinity, with departures of ~0.2 kg/m³ (Sirota et al., 2016). The shape of the vertical temperature profile, with the thermocline at ~25-m depth, turns from a smooth curve in early summer that exhibits a gradual transition over ~15 m into a sequence of distinct steps (without temperature and/or salinity inversions) by midsummer (thermohaline staircases), which further merge into a single sharp step, with a transitional layer <2 m thick in late summer (Arnon et al., 2016) (Figure 2c). The onset of the thermohaline staircase is accompanied by an increase in the maximum vertical temperature gradient across the thermocline, from 0.6°C/m to 9°C/m (Figure 3b). The downward salt flux sharply increases during the summer, exceeding 1 kg/day/m² during late summer (Arnon et al., 2016), twice the effective surface salt flux due to evaporation. The onset of thermohaline staircases in midsummer, as well as the associated increase in the salt flux, coincides with the drop of the density ratio, R_{ρ} below 2 (Figure 3b).

The spatial variations in the thermohaline stratification mirror the seasonal evolution (Figures 3d-3g). The freshwater inflows lower the surface salinity in the northern part of the lake, so that the surface salinity increases toward the drier, southern part of the lake (Figure 3d). Consequently, the salinity difference between the upper and lower layers grows from 2.02 kg/m³ in the north to 2.47 kg/m³ at the southern end (Figure 3e). Even though the temperature difference between the epilimnion and hypolimnion is uniform across sites, ~9°C in July (Figure 3h), corresponding to a density difference of ~4 kg/m³, the profile shapes vary drastically. While the northern profiles exhibit a gradual transition layer with thickness of ~25 m (centered at ~25-m depth), coevally, the southern profiles display a much thinner <5-m-thick transitional layer characterized by thermohaline staircases (Figures 3h and 3i). As a result of this thermocline sharpening, the maximum vertical temperature gradient increases southward from 1°C/m to 8°C/m (Figures 3f and 3i). The halite crystallization rate below the thermocline, which reflects the preferred downward transport of salt over heat by double-diffusive convection from the epilimnion to the hypolimnion (Ouillon et al., 2019; Sirota et al., 2016), doubles from 0.2 mm/day in the northern part to 0.4 mm/day in the south (Figure 3j and the supporting information). At no location did we observe halite to crystallize above the thermocline, as increasing temperature and downward double-diffusive salt flux leave the epilimnion undersaturated (Arnon et al., 2016; Sirota et al., 2016). The southward increase in the double-diffusive salt flux is consistent with the observed decrease of the density ratio R_{ρ} from 2.4 to 1.5 (Figure 3g). The region where $R_{\rho} < 2$ exhibits thermohaline staircases, increased downward salt flux, and sharpening of the vertical temperature profiles, thus consistent with double-diffusive convection theory.

Figure 4 compiles the seasonal and regional variations of the thermohaline stratification parameters into comprehensive spatiotemporal diagrams (grid data in supporting information Table S1). These allow us to identify the physical mechanisms that govern the various regions of the

SIROTA ET AL. 6 of 10



Dead Sea throughout the year, due to the continuous lake level decline (Figure 4a) and the southward drying trend (Figure 4b). The salinity difference between epilimnion and hypolimnion increases until it peaks in late summer, and it is larger toward the south (Figure 4b). The corresponding temperature difference grows during the buildup of the summer stratification, followed by late summer cooling, with little variation along the north-south transect (Figure 4c). Interestingly, the density ratio, R_{ρ} , decreases monotonically toward the drier region and season (Figure 4d), even though the salinity and temperature differences individually peak in midsummer. This reflects the different rates at which the temperature and salinity differences change during early and late summer, that is, during the warming and cooling periods, as a result of the external heat forcing by the atmosphere. The reduced density ratio is strongly correlated with the seasonal and regional sharpening of the thermocline (Figure 4e) and the transition from rounded profiles to thermohaline staircases and eventually a single sharp step (Figure 4f). Consistent with these observations, lower values of R_{ρ} are also associated with larger downward salt fluxes (Figure 3j). While in the northern region and during early summer only the basic double-diffusive fingering instability is active $(2 < R_{\rho} < \frac{1}{2})$, the γ instability is excited in the southern region and during late summer $(1 < R_{\rho} < 2)$ and staircases occur. Accordingly, thermohaline sharpening in the staircase regime leads to increased turbulent salt and heat fluxes at R_{ρ} < 2 while maintaining the heat to salt flux ratio below unity (Traxler et al., 2011), thus explaining the increasing rates of halite crystallization southward (Figure 3j). The decrease in the salinity difference during late summer (Figures 3a and 4b) is attributed to the downward flux of dissolved salt from the epilimnion to the hypolimnion, which maintains undersaturation above the thermocline while promoting halite deposition below.

Based on the above field data and their analysis, we propose that the regional hydroclimate governs the distribution of halite deposits on the lake floor by generating regional and seasonal variations in the density ratio, R_p . The density ratio, in turn, controls where and when thermohaline staircases appear and merge (Figures 4d–4f), thereby enhancing the local downward salt flux and increasing halite deposition in these regions. This process also explains the "halite focusing" mechanism (Sirota et al., 2018), which causes amplified halite thickness at the basin depocenter at the expense of coexisting marginal halite dissolution, and increased deposition rates in the saltier regions of the lake, away from the influence of freshwater inflows (Figures 1b and 2a).

3.2. Origin, Length, and Time Scales of the Layering Instability

The variations of the thermohaline staircases in time and space follow variations in the density ratio, consistent with γ instability theory. These staircases show monotonic decrease in the temperature (and salinity) with depth (Figure 3h; Arnon et al., 2016; Sirota et al., 2016), unlike staircases associated with thermohaline intrusions due to lateral sheared advection across lateral water mass gradients, characterized by inversions in temperature and salinity with depth (Ruddick et al., 1999; Ruddick & Kerr, 2003; Ruddick & Richards, 2003; Simeonov & Stern, 2004, 2007). Basic scaling considerations (Radko, 2013) indicate that the most unstable salt fingering mode in the Dead Sea has a horizontal wavelength of O(5 cm). Direct numerical simulations (DNS) (Stellmach et al., 2011) demonstrate that the vertical wavelength of the first emerging horizontal layers, for conditions typical of the Dead Sea, is about 1 order of magnitude larger than this horizontal wavelength of the dominant salt fingering mode, so that we expect the first thermohaline staircases to appear with a thickness of O(50 cm). Additional DNS results (Traxler et al., 2011) indicate that under the general conditions prevailing in the Dead Sea, the amplitude of the layering mode takes O(10 min) to grow by an order of magnitude at $R_{\rho} = 2$, and O(1 min) at $R_{\rho} = 1.5$. Successive merging events then lead to the formation of increasingly thick layers associated with increased turbulent fluxes, as observed in Figure 3j. While these scales do not directly translate into an estimate of the time required for large-amplitude staircases to form, they indicate that the γ instability grows sufficiently fast to enable the emergence of thermohaline staircases in the Dead Sea, which are observed to evolve over a period of days to weeks. Furthermore, the marked acceleration of growth associated with a decrease of the density ratio from 2 to 1.5 is consistent with the observed spatiotemporal sharpening of the staircases (Figure 4).

3.3. Implications for "Salt Giants"

Following decades of research into the accretion of salt giants in the geological record (Dyni, 1996; Garcia-Veigas et al., 1995; Hardie & Lowenstein, 2004; Hsü et al., 1973; Roveri, Manzi, et al., 2014; Simon & Meijer, 2017), their spatial halite thickness variations, that is, the absence of halite from the margins of

SIROTA ET AL. 7 of 10



deep basins with enormous depocenter halite, remain enigmatic (Roveri, Manzi, et al., 2014). This has motivated investigations into the vertical and horizontal salinity distributions in hypersaline waterbodies (Karakitsios et al., 2017; Meijer & Krijgsman, 2005; Roveri, Flecker, et al., 2014; Simon & Meijer, 2017); so far, their quantification has proved challenging. Here we provide a novel perspective of the oceanography/limnology mechanisms that can translate simple surface evaporation into drastically nonuniform halite deposition across basin; this is based on variations in double-diffusive convection and secondary instabilities resulting in staircases formation. This mechanism can now explain the enigmatic geological observations. The explanation is based on regional and seasonal variations in the transfer of dissolved salt from the saltier epilimnion, where evaporation occurs, to the hypolimnion, where thick halite is deposited on the basin floor. Regional surface salinity gradients and the associated vertical salinity distributions are determined by the location and intensity of freshwater inflows, which in turn control the properties of the stratified water column and the intensity of the downward transport of salt. Together, these accelerate deposition rate at deeper and drier regions of the basin that lead to thickness variations in the halite unit and control the extent of truncation surfaces, which observed in the geological record of deep hypersaline basins. The quantitative analysis presented here can be applied for reconstructing the paleo-oceanography/limnology of past hypersaline environments and their paleohydroclimatologic controls.

4. Summary and Conclusions

By in situ observations from the only modern analog on Earth, we determine how large-scale salt deposits have accreted in deep hypersaline basins. We directly observe how hydroclimatic forcing, during dry stages, affect thermohaline stratification, characterized by stabilizing thermocline and destabilizing halocline, leading to the emergence of double diffusion salt fingers $(R_{\rho} < \frac{1}{r})$ transferring dissolved salts to the lower waterbody. Further drying, seasonally or spatially, results in reducing R_{ρ} toward unity leading to the formation of vertical thermohaline staircases, as an expression for the growth of the secondary mean-field γ instability. The formation of staircases is associated with dramatic increase of turbulent heat and salt fluxes, followed by staircases merging and coalescing into a single sharp temperature and salinity step, which further increase the downward salt flux and accelerate accumulation of salt deposits. Numerical analysis shows that the time span for the formation of thermohaline staircases becomes shorter with decreasing stability ratio, promoting downward salt fingering flux and halite deposition. The double-diffusive convection is strengthened, (i) during the dry summer, as water evaporates from the lake, and (ii) along the surface salinity gradient, from the freshwater inflows to the drier and saltier zones of the lake. Regional hydroclimatic gradients dictates thickening of salt deposits toward the drier areas, and the vertical transport of dissolved salt dictates thicker deposits in the deep parts of the basins; thus, these drivers generate regionally uneven thickness of salt deposits. These spatial variations in halite deposition can explain observed characteristics of "salt giants," where thick halite sequences were deposited at high rates and are observed in basins' depocenter and away from diluted discharges.

Acknowledgments

Hallel Lutzki, Raanan Bodzin, Assaf Mor, Haggai Eyal, and the R/V Taglit team are acknowledged for field assistance. This study was funded by the Israel Science Foundation, PI-NGL (grant # ISF-1471/18) and PI-YE (grant # ISF-946/18), U.S.-Israel Binational Science Foundation, PI-NGL grant # BSF-2018/035, through a joint National Science Foundation-U.S.-Israel Binational Science Foundation program (grant # NSF-1936358 PI-EM and grant # BSF-2019/637 PI-NGL), by the Army Research Office under grant # W911NF-18-1-0379, PI-EM, and by the U.S.-Israel Binational Science Foundation (BSF) Prof. Rahamimoff Travel Grant for Young Scientists to Ido Sirota (grant # 0378745).

Data Availability Statement

Field measurements are presented in Table S1 in the supporting information, Dead Sea level and meteorological data were obtained from http://www.water.gov.il and https://ims.gov.il/, respectively.

References

Anati, D. A., & Stiller, M. (1991). The post-1979 thermohaline structure of the Dead Sea and the role of double-diffusive mixing. *Limnology and Oceanography*, 36(2), 342–353. https://doi.org/10.4319/lo.1991.36.2.0342

Anati, D. A., Stiller, M., Shasha, S., & Gat, J. R. (1987). Changes in the thermo-haline structure of the Dead Sea: 1979–1984. Earth and Planetary Science Letters, 84(1), 109–121. https://doi.org/10.1016/0012-821X(87)90181-6

Arnon, A., Selker, J. S., & Lensky, N. G. (2016). Thermohaline stratification and double diffusion diapycnal fluxes in the hypersaline Dead Sea. *Limnology and Oceanography*, 61(4), 1214–1231. https://doi.org/10.1002/lno.10285

Dyni, J. R. (1996). Sodium carbonate resources of the Green River Formation. *US Geological Survey* (Vol. US Geologi). Retrieved from https://pubs.usgs.gov/of/1996/ofr-96-0729/ofr-96-0729.pdf

Flecker, R., Krijgsman, W., Capella, W., de Castro Martíns, C., Dmitrieva, E., Mayser, J. P., et al. (2015). Evolution of the Late Miocene Mediterranean-Atlantic gateways and their impact on regional and global environmental change. *Earth-Science Reviews*, 150, 365–392. https://doi.org/10.1016/j.earscirev.2015.08.007

SIROTA ET AL. 8 of 10



- Garcia-Veigas, J., Orti, F., Rosell, L., Ayora, C., Rouchy, J.-M., & Lugli, S. (1995). The Messinian salt of the Mediterranean: Geochemical study of the salt from the Central Sicily Basin and comparison with the Lorca Basin (Spain). *Bulletun-Societe Geologique De France*, 166, 699–710.
- Gavrieli, I., Lensky, N., Abelson, M., Aharon, O., Brenner, S., Lensky, I., et al. (2011). Red Sea to Dead Sea water conveyance (RSDSC) study: Dead Sea research team (Rep. GSI/10/2011). Israel, Jerusalem: Geological Survey of Israel. https://doi.org/10.13140/RG.2.2.24893.72164
- Gertman, I., & Hecht, A. (2002). The Dead Sea hydrography from 1992 to 2000. Journal of Marine Systems, 35(3–4), 169–181. https://doi.org/10.1016/S0924-7963(02)00079-9
- Gertman, I., Kress, N., Katsenelson, B., & Zavialov, P. (2010). Equations of state for the Dead Sea and Aral Sea: Searching for common approaches, Israel Oceanographic and Limnological Research (IOLR) Report IOLR/12/2010.
- Hardie, L. A., & Lowenstein, T. K. (2004). Did the Mediterranean Sea dry out during the Miocene? A reassessment of the evaporite evidence from DSDP legs 13 and 42A cores. *Journal of Sedimentary Research*, 74(4), 453–461. https://doi.org/10.1306/ 112003740453
- Hsu, K. J. (1972). Origin of saline giants: A critical review after the discovery of the Mediterranean evaporite. Earth Science Reviews, 8(4), 371–396. https://doi.org/10.1016/0012-8252(72)90062-1
- Hsü, K. J., Ryan, W. B. F., & Cita, M. B. (1973). Late Miocene desiccation of the Mediterranean. Nature, 242(5395), 240–244. https://doi.org/10.1038/242240a0
- Karakitsios, V., Cornée, J. J., Tsourou, T., Moissette, P., Kontakiotis, G., Agiadi, K., et al. (2017). Messinian salinity crisis record under strong freshwater input in marginal, intermediate, and deep environments: The case of the North Aegean. *Palaeogeography*, *Palaeoclimatology*, *Palaeoecology*, 485, 316–335. https://doi.org/10.1016/j.palaeo.2017.06.023
- Kirkham, C., Bertoni, C., Cartwright, J., Lensky, N. G., Sirota, I., Rodriguez, K., & Hodgson, N. (2020). The demise of a 'salt giant' driven by uplift and thermal dissolution. Earth and Planetary Science Letters, 531, 115933. https://doi.org/10.1016/j.epsl.2019.115933
- Kozary, M. T., Dunlap, J. C., & William, H. E. (1968). Incidence of saline deposits in geologic time. In R. B. Mattox et al. (Eds.), Saline deposits: A symposium based on papers from the international conference on saline deposits (Vol. 88, pp. 43–57). Houston: Geological Society of America Special Paper.
- Lensky, N. G., Dvorkin, Y., Lyakhovsky, V., Gertman, I., & Gavrieli, I. (2005). Water, salt, and energy balances of the Dead Sea. Water Resources Research, 41, W12418. https://doi.org/10.1029/2005WR004084
- Lowenstein, T. K., & Hardie, L. A. (1985). Criteria for the recognition of salt-pan evaporites. Sedimentology, 32(5), 627-644.
- Meijer, P., & Krijgsman, W. (2005). A quantitative analysis of the desiccation and re-filling of the Mediterranean during the Messinian salinity crisis. Earth and Planetary Science Letters, 240(2), 510–520. https://doi.org/10.1016/j.epsl.2005.09.029
- Mor, Z., Assouline, S., Tanny, J., Lensky, I. M., & Lensky, N. G. (2018). Effect of water surface salinity on evaporation: The case of a diluted buoyant plume over the Dead Sea. Water Resources Research, 54, 1460–1475. https://doi.org/10.1002/2017WR021995
- Ouillon, R., Lensky, N. G., Lyakhovsky, V., Arnon, A., & Meiburg, E. (2019). Halite precipitation from double-diffusive salt fingers in the Dead Sea: Numerical simulations. Water Resources Research, 55, 4252–4265, https://doi.org/10.1029/2019WR024818
- Radko, T. (2003). A mechanism for layer formation in a double-diffusive fluid. *Journal of Fluid Mechanics*, 497(497), 365–380. https://doi.org/10.1017/S0022112003006785
- Radko, T. (2013). Double-diffusive convection. Cambridge: Cambridge University Press. https://doi.org/10.1017/CBO9781139034173 Ronov, A. B., Khain, V. E., Balukhovsky, A. N., & Seslavinsky, K. B. (1980). Quantitative analysis of Phanerozoic sedimentation.
- Sedimentary Geology, 25(4), 311–325. https://doi.org/10.1016/0037-0738(80)90067-6
 Roveri, M., Manzi, V., Bergamasco, A., Falcieri, F. M., Gennari, R., Lugli, S., & Schreiber, B. C. (2014). Dense shelf water cascading and
- Messinian canyons: A new scenario for the Mediterranean salinity crisis. *American Journal of Science*, 314(3), 751–784. https://doi.org/10.2475/05.2014.03
- Roveri, M., Flecker, R., Krijgsman, W., Lofi, J., Lugli, S., Manzi, V., et al. (2014). The Messinian salinity crisis: Past and future of a great challenge for marine sciences. *Marine Geology*, 352, 25–58. https://doi.org/10.1016/j.margeo.2014.02.002
- Ruddick, B., & Richards, K. (2003). Oceanic thermohaline intrusions: Observations. *Progress in Oceanography*, 56, 499–527. https://doi.org/10.1016/S0079-6611(03)00028-4
- Ruddick, B. R., & Turner, J. S. (1979). The vertical length scale of double-diffusive intrusions. Deep Sea Research Part A, Oceanographic Research Papers, 26(8), 903–913. https://doi.org/10.1016/0198-0149(79)90104-3
- Ruddick, B., & Kerr, O. (2003). Oceanic thermohaline intrusions: Theory. Progress in Oceanography, 56, 483–497. https://doi.org/10.1016/ S0079-6611(03)00029-6
- Ruddick, B. R., Phillips, O. M., & Turner, J. S. (1999). A laboratory and quantitative model of finite-amplitude thermohaline intrusions. Dynamics of Atmospheres and Oceans, 30(2–4), 71–99. https://doi.org/10.1016/S0377-0265(99)00021-4
- Schmalz, R. F. (1969). Deep-water evaporite deposition: A genetic model. *AAPG Bulletin*, 53(4), 798–823. https://doi.org/10.1306/5D25C7FD-16C1-11D7-8645000102C1865D
- Schmitt, R. W. (1981). Form of the temperature-salinity relationship in the central water: Evidence for double-diffusive mixing. *Journal of Physical Oceanography*, 11(7), 1015–1026.
- Simeonov, J., & Stern, M. (2004). Double-diffusive intrusions on a finite-width thermohaline front. *Journal of Physical Oceanography*, 34(7), 1723–1740. https://doi.org/10.1175/1520-0485(2004)034%3c1723:DIOAFT%3e2.0.CO;2
- Simeonov, J., & Siern, M. E. (2007). Equilibration of two-dimensional double-diffusive intrusions. *Journal of Physical Oceanography*, 37(3), 625–643. https://doi.org/10.1175/JPO3000.1
- Simon, D., & Meijer, P. T. (2017). Salinity stratification of the Mediterranean Sea during the Messinian crisis: A first model analysis. *Earth and Planetary Science Letters*, 479, 366–376. https://doi.org/10.1016/j.epsl.2017.09.045
- Sirota, I., Arnon, A., & Lensky, N. G. (2016). Seasonal variations of halite saturation in the Dead Sea. Water Resources Research, 52, 7151–7162. https://doi.org/10.1002/2016WR018974.Received
- Sirota, I., Enzel, Y., & Lensky, N. G. (2017). Temperature seasonality control on modern halite layers in the Dead Sea: In situ observations. Geological Society of America Bulletin, 129(9–10), 1181–1194. https://doi.org/10.1130/B31661.1
- Sirota, I., Enzel, Y., & Lensky, N. G. (2018). Halite focusing and amplification of salt layer thickness: From the Dead Sea to deep hypersaline basins. *Geology*, 46(10), 851–854. https://doi.org/10.1130/G45339.1
- Steinhorn, I. (1983). In situ salt precipitation at the Dead Sea. Limnology and Oceanography, 28(3), 580–583. https://doi.org/10.4319/lo.1983.28.3.0580
- Steinhorn, I. (1985). The disappearance of the long term meromictic stratification of the Dead Sea. *Limnology and Oceanography*, 30(3), 451–472.

SIROTA ET AL. 9 of 10



- Stellmach, S., Traxler, A., Garaud, P., Brummell, N., & Radko, T. (2011). Dynamics of fingering convection. Part 2. The formation of thermohaline staircases. *Journal of Fluid Mechanics*, 677, 554–571. https://doi.org/10.1017/jfm.2011.99
- Stern, M. E. (1960). The "salt-fountain" and thermohaline convection. *Tellus*, 12(2), 172–175. https://doi.org/10.1111/j.2153-3490.1960. tb01295.x
- Stiller, M., Gat, J. R., & Kaushansky, P. (1997). Halite precipitation and sediment deposition as measured in sediment trapsdeployed in the Dead Sea: 1981–1983. In T. M. Niemi, Z. Ben-Avraham, & J. R. Gat (Eds.), *The Dead Sea: The lake and its settings* (pp. 171–183). Oxford: Oxford University Press.
- Traxler, A., Stellmach, S., Garaud, P., Radko, T., & Brummell, N. (2011). Dynamics of fingering convection. Part 1. Small-scale fluxes and large-scale instabilities. *Journal of Fluid Mechanics*, 677, 530–553. https://doi.org/10.1017/jfm.2011.98
- Turner, J. S. (1974). Double-diffusive phenomena. Annual Review of Fluid Mechanics, 6, 37-54.
- Warren, J. K. (2010). Evaporites through time: Tectonic, climatic and eustatic controls in marine and nonmarine deposits. *Earth-Science Reviews*, 98(3–4), 217–268. https://doi.org/10.1016/j.earscirev.2009.11.004
- Zodiatis, G., & Gasparini, G. P. (1996). Thermohaline staircase formations in the Tyrrhenian Sea. Deep-Sea Research Part I: Oceanographic Research Papers, 43(5), 655–678. https://doi.org/10.1016/0967-0637(96)00032-5

SIROTA ET AL. 10 of 10